Available online at www.sciencedirect.com

SciVerse ScienceDirect

Ceramics International 38 (2012) 2609–2612

CERAMICS INTERNATIONAL

www.elsevier.com/locate/ceramint

Short communication

Size–strain line broadening analysis of high-permittivity oxynitrides $BaTaO_2N$ and $BaNbO_2N$

Young-Il Kim *

Department of Chemistry, Yeungnam University, Gyeongsan 712-749, Republic of Korea

Received 17 May 2011; accepted 27 October 2011
Available online 4 November 2011

Abstract

X-ray line broadening analysis of polycrystalline $BaTaO_2N$ and $BaNbO_2N$ was performed to extract microstructural information beyond the average structural descriptions. Both $BaTaO_2N$ and $BaNbO_2N$ display markedly broader diffraction peak profiles than observed from an oxide analogue $KTaO_3$. Examination of the angular dependence of the integral peak breadth shows that the line broadening of $BaTaO_2N$ is caused by both finite crystallite size (D_v = 117 nm) and micro-strain (ε = 0.038%), whereas the latter effect dominates in the case of $BaNbO_2N$ (D_v = 574 nm, ε = 0.11%). The above results indicate that the temperature-independent high-permittivity behavior of $BaTaO_2N$ arises due to local atomic displacements, and further imply that even stronger dielectric polarizations could be generated in $BaNbO_2N$.

Keywords: B. X-ray methods; B. Grain size; D. Perovskites

1. Introduction

Being comparable in size, charge, and electronegativity, the two anions O^{-2} and N^{-3} have similar bonding preferences and can form oxynitride type mixed anion compounds. As the coexistence of O^{-2} and N^{-3} in the anion sub-lattice gives rise to physical and chemical properties clearly distinct from those of either the pure oxide or the pure nitride relatives, the oxynitrides are regarded a promising system for exploring unconventional material performances. In fact, there have been considerable research efforts in the past decade to develop novel functional materials using various transition metal oxynitrides [1–4]. As an example, the perovskite $BaTaO_2N$ was reported to exhibit unusually high and temperature-independent dielectric constants (κ) both in polycrystalline ($\kappa \approx 5000$ at 180–300 K) and thin film ($\kappa \approx 220$ at 4–300 K) forms [3,5]. Interestingly $BaTaO_2N$ has an average crystal structure of primitive cubic symmetry, which is seemingly inconsistent with high-κ behavior. Later studies, however, revealed that the $BaTaO_2N$ lattice contains substantial local distortions and is largely deviated from the ideal cubic geometry [6–8]. Such a local structural phenomenon is believed to derive from the random O/N distribution in the anion sub-lattice, coupled with the inequity of Ta–O and Ta–N bonds.

In order for better utilizing the dielectric property of $BaTaO_2N$, it is of crucial importance to comprehend the nature of the lattice polarization. In this regard, we examined the microstructural aspects of $BaTaO_2N$, in comparison with other cubic perovskites $BaNbO_2N$ and $KTaO_3$, by powder diffraction line profile analysis (LPA) based on the simplified integral breadth method. Since the earlier recognition by Scherrer of the dependence of diffraction line width on crystallite size [9], diffraction LPA has been widely used for studying microstructural characteristics, *i.e.* size and strain, of various extended solids [10]. While there are known several different LPA schemes in practice, integral breadth methods are frequently used for quick assessment of the size–strain line broadening effects that are caused by the finite size of the coherently scattering domains and by lattice strain [11]. As is clearly found from the present LPA and electron microscopy, $BaTaO_2N$ and $BaNbO_2N$ are formed from much smaller crystallites and with larger micro-strains than the oxide $KTaO_3$. Moreover it is revealed that $BaNbO_2N$ contains larger crystallites and larger strain than $BaTaO_2N$.

2. Experimental

Powder samples of $BaTaO_2N$ and $BaNbO_2N$ were prepared by ammonolysis reactions using $BaCO_3$ (Aldrich, 99.98%), Ta_2O_5 (Aldrich, 99.99%), and Nb_2O_5 (Aldrich, 99.99%). For each composition, a stoichiometric mixture of powder reagents

* Tel.: +82 53 810 2353; fax: +82 53 810 4613.
E-mail address: yikim@ynu.ac.kr.

0272-8842/$36.00
doi:10.1016/j.ceramint.2011.10.078

was heated at 1273 K for a total of 60 h with intermittent grinding, in an ammonia flow of ≈50 sccm. A reference oxide $KTaO_3$ was also prepared from a stoichiometric mixture of K_2CO_3 (Alfa-Aesar, 99.0%) and Ta_2O_5 (Aldrich, 99.99%) by heat treatment in air at 1273 K for 60 h.

Synchrotron powder X-ray diffraction (XRD) data were collected at 295 K, on a high-resolution powder diffractometer (BL-8C2) installed at Pohang Accelerator Laboratory (PAL) in Korea. The use of high-resolution synchrotron radiation (λ = 1.550 Å) helped to minimize any instrumental contributions to the line broadening effect. A standard reference material, LaB_6 (NIST SRM 660a, a = 4.156468 Å) [12], was employed for wavelength calibration and also for correcting instrumental broadening of line widths. Diffraction profiles were recorded over the 2θ range 10–130° with a step size of 0.01° for $BaTaO_2N$, $BaNbO_2N$, and $KTaO_3$, and 0.002° for LaB_6. The sample holder was spun at 60 rpm in the Bragg–Brentano configuration.

The grain sizes and morphologies of the sample powders were examined using field-emission scanning electron microscopes (Hitachi, S-4800 and S-4200). SEM powder samples were mounted on aluminum stubs using double-sided conductive carbon tabs, and coated with Pt prior to imaging.

3. Results and discussion

Synchrotron XRD profiles of $BaTaO_2N$, $BaNbO_2N$, $KTaO_3$, and LaB_6 are presented in Fig. 1. The four patterns commonly correspond to the simple cubic lattice, without any indication of peak splitting or any impurity phases. Rietveld refinement confirmed that all the samples belong to the $Pm\bar{3}m$ space group with lattice parameters of 4.11225(2) Å, 4.12131(3) Å, and 3.98849(3) Å for $BaTaO_2N$, $BaNbO_2N$, and $KTaO_3$, respectively. Each sample presented 14–22 diffraction peaks at $2\theta < 130°$ ($d > 0.86$ Å), for which the full width at half maximum (Γ, Fig. 2a) and the Lorentz fraction (η) were determined by fitting a pseudo-Voigt function. Subsequently the integral breadth (β) was calculated using the equation [13]:

$$\beta = \frac{\Gamma}{2}\left\{\sqrt{\frac{\pi}{\ln 2}} + \eta\left(\pi - \sqrt{\frac{\pi}{\ln 2}}\right)\right\}$$

After correcting for the instrumental broadening, β_{inst}, with LaB_6 as a reference, Williamson–Hall (W–H) plots [14] for $KTaO_3$, $BaTaO_2N$, and $BaNbO_2N$ were constructed based on the function:

$$(\beta_i - \beta_{inst})\cos\theta_i = \frac{\lambda}{D_v} + 4\varepsilon \sin\theta_i$$

where β_i is the integral breadth (in radians 2θ) of the ith Bragg reflection positioned at $2\theta_i$ and λ is the radiation wavelength. The slope and ordinate intercept of the W–H plot (Fig. 2b) were used to quantify crystallite size (D_v) and strain (ε) contributions to the peak broadening.

Although the three perovskite samples were prepared using the same sintering temperature and time, the resulting microstructural characteristics turned out to be quite distinct. While $KTaO_3$ consists of crystallites in the micron range with

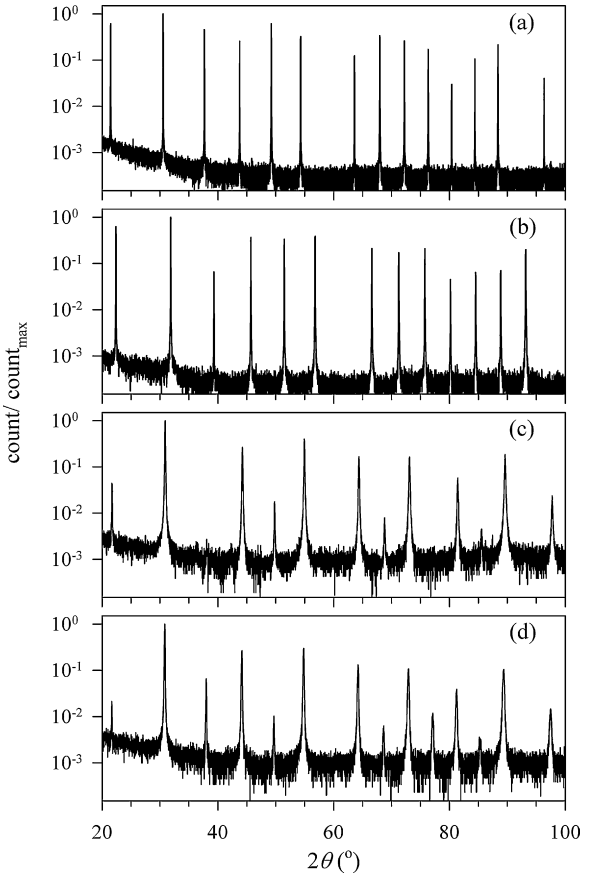

Fig. 1. Synchrotron XRD (λ = 1.550 Å) patterns for (a) LaB_6, (b) $KTaO_3$, (c) $BaTaO_2N$, and (d) $BaNbO_2N$.

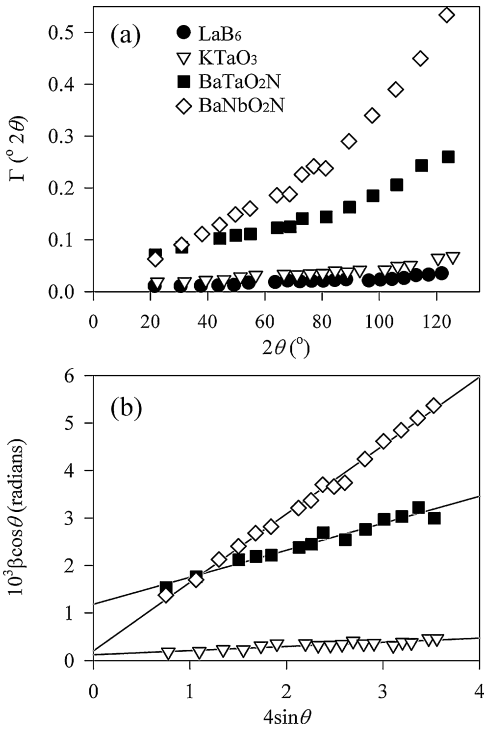

Fig. 2. (a) Peak widths (Γ) for LaB_6, $KTaO_3$, $BaTaO_2N$, and $BaNbO_2N$, and (b) the corresponding Williamson–Hall plots. The same legend symbols are used for both panels.

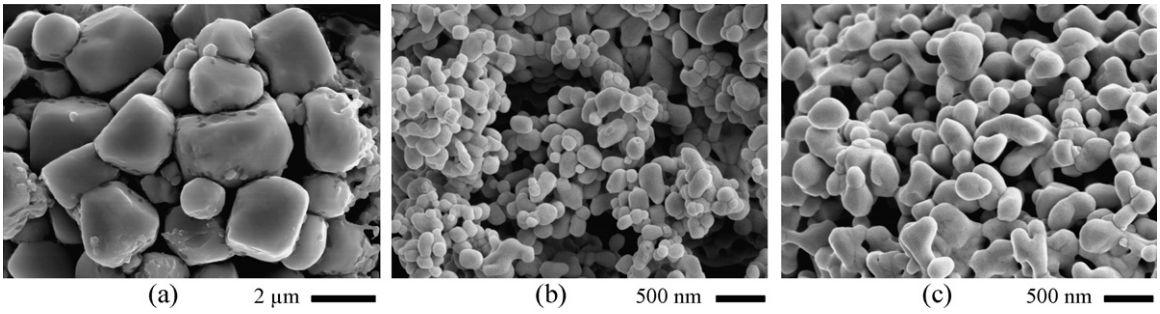

Fig. 3. SEM images of (a) $KTaO_3$, (b) $BaTaO_2N$, and (c) $BaNbO_2N$.

minimal strain (D_v = 1034 nm, ε = 0.005%), both oxynitride samples have markedly smaller crystallite sizes and larger strains ($BaTaO_2N$: D_v = 117 nm, ε = 0.038%; $BaNbO_2N$: D_v = 574 nm, ε = 0.11%). The crystallite size and strain are directly affected by the degree of crystal imperfection. That is, the higher concentration of lattice defects should reduce the crystallite size while increasing the strain. The present LPA shows that the two oxynitride type samples are more defective than the oxide example $KTaO_3$. The better sintering of the latter, compared with the two oxynitrides, may be partly due to the flux behavior of the alkali component, and also to the generic refractory nature of the nitride-containing phases. Additionally, it should be mentioned that the intrinsic local structural distortion in oxynitrides contributes to develop substantial amounts of micro-strain within the crystallites. Recent experimental investigations using extended X-ray absorption fine structure [6], pair-distribution-functions [7], and electron diffraction [8] have elucidated that $BaTaO_2N$ consists of irregularly distorted TaO_4N_2 octahedra, which must have a profound impact on the lattice strain. It is highly probable that such a structural feature exists universally in the oxynitride perovskite system, and we regard the size–strain line broadening of oxynitride perovskites as being associated with compositional aspects and structural disorders as well.

An interesting finding is that both the crystallite size and strain are assessed as being significantly larger for $BaNbO_2N$ than for $BaTaO_2N$. Taking into account that the niobium-related phases tend to melt at lower temperatures than their tantalum analogues (Ta: 3290 K; Nb: 2750 K; Ta_2O_5: 2145 K; Nb_2O_5: 1785 K), it is duly expected that $BaNbO_2N$ would have a lower melting point than $BaTaO_2N$ and would undergo faster crystallite growth. However the larger strain of $BaNbO_2N$ is not explainable by the above reasoning, but is attributable to the more pronounced local structural disorder, as described below.

For $BaTaO_2N$, the packing incompatibility was pointed out as a plausible origin of the local atomic displacements [8]. The perovskite tolerance factor for the composition $BaTaO_2N$ is calculated as 1.04, which practically means that the size of a Ta^{+5} ion is too small to fit the octahedral cavity. Accordingly, the bond valence sum (BVS) calculations [15] for the average structure of $BaTaO_2N$ reveal a notable underbonding of the Ta ion. Using the software VALENCE [16], we obtain +2.71 valence units (v.u.) for Ba, +4.54 v.u. for Ta, −2.13 v.u. for O, and −2.99 v.u. for N ions, and subsequently a global instability index (GII) of 0.388 for $BaTaO_2N$. A GII value exceeding 0.2 is generally considered unrealistic for any standard state structures [15], and this BVS calculation itself can be a strong implication of structural relaxation in $BaTaO_2N$. Previously it was rationalized that such an unfavorable bonding geometry of $BaTaO_2N$ can be alleviated by the displacement of Ta ions away from the ideal high-symmetry site [8]. Similarly for the average structure of $BaNbO_2N$, the BVS calculation yields +2.67 v.u. for Ba, +4.41 v.u. for Nb, −2.10 v.u. for O, and −2.95 v.u. for N ions, and a GII of 0.402. Here the bond valence of the octahedral cation and the GII for $BaNbO_2N$ deviate from their respective ideal values, even farther than in $BaTaO_2N$. This leads us to the deduction that $BaNbO_2N$ would contain more prominent lattice disorders than $BaTaO_2N$. It is also noteworthy that Nb, being more electronegative than Ta, is more prone to intra-octahedral distortions *via* second-order Jahn–Teller distortions [17,18]. We regard LPA results as corroborating the above assumptions well.

The crystallite morphologies and sizes of $KTaO_3$, $BaTaO_2N$, and $BaNbO_2N$ are compared using SEM in Fig. 3. Although the crystallite sizes are somewhat distributed in all three cases, the majority of the observed crystallites fall in to size ranges roughly corresponding to the LPA result: 1–3 μm for $KTaO_3$, 80–300 nm for $BaTaO_2N$, and 300–500 nm for $BaNbO_2N$. It is noted that the particulates of $KTaO_3$ maintain cube-like polyhedral shapes whereas those of $BaTaO_2N$ and $BaNbO_2N$ have rather curvy surfaces. The loss of crystal habits in the above oxynitride powders is indicative of the lack of long-range lattice periodicity, namely the prevalence of irregular structural distortions in local scales. Such a morphological characteristic is in accordance with the presence of large micro-strains. In view of the dielectric property, the larger strain of $BaNbO_2N$ gives promises as a new high-κ material.

4. Conclusions

By X-ray line broadening analysis, it was demonstrated that the oxynitrides $BaTaO_2N$ and $BaNbO_2N$ are formed with smaller crystallite sizes and greater micro-strains than the oxide analogue $KTaO_3$. It is judged that the micro-strains of the above oxynitrides stem largely from the local atomic displacements, which has immediate relevance to the dielectric behavior. Based on the present LPA results, the unusual dielectric properties of the simple cubic perovskite $BaTaO_2N$ can be attributed to the local polarizations induced by geometry

relaxation. Furthermore, $BaNbO_2N$ is identified as a promising high-permittivity candidate.

Acknowledgements

This work was supported by National Nuclear R&D Program (2010-0018525) and Basic Science Research Program (2010-0008039) through the National Research Foundation of Korea.

References

[1] M. Jansen, H.P. Letschert, Inorganic yellow-red pigments without toxic metals, Nature 404 (2000) 980–982.
[2] M. Higashi, R. Abe, T. Takata, K. Domen, Photocatalytic overall water splitting under visible light using $ATaO_2N$ (A = Ca, Sr, Ba) and WO_3 in a IO_3^-/I^- shuttle redox mediated system, Chem. Mater. 21 (2009) 1543–1549.
[3] Y.-I. Kim, P.M. Woodward, K. Baba-Kishi, C.-W. Tai, Characterization of the structural, optical, and dielectric properties of oxynitride perovskites AMO_2N (A = Ba, Sr Ca; M = Ta, Nb), Chem. Mater. 16 (2004) 1267–1276.
[4] A.B. Jorge, J. Oro-Sole, A.M. Bea, N. Mufti, T.T.M. Palstra, J.A. Rodgers, J.P. Attfield, A. Fuertes, Large coupled magnetoresponses in $EuNbO_2N$, J. Am. Chem. Soc. 130 (2008) 12572–12573.
[5] Y.-I. Kim, W. Si, P.M. Woodward, E. Sutter, S. Park, T.T. Vogt, Epitaxial thin-film deposition and dielectric properties of the perovskite oxynitride $BaTaO_2N$, Chem. Mater. 19 (2007) 618–623.
[6] B. Ravel, Y.-I. Kim, P.M. Woodward, C.M. Fang, Role of local disorder in the dielectric response of $BaTaO_2N$, Phys. Rev. B 73 (2006) 184121.
[7] K. Page, M.W. Stoltzfus, Y.-I. Kim, T. Proffen, P.M. Woodward, A.K. Cheetham, R. Seshadri, Local atomic ordering in $BaTaO_2N$ studied by neutron pair distribution function analysis and density functional theory, Chem. Mater. 19 (2007) 4037–4042.
[8] R.L. Withers, Y. Liu, P.M. Woodward, Y.-I. Kim, Structurally frustrated polar nanoregions in $BaTaO_2N$ and the relationship between its high dielectric permittivity and that of $BaTiO_3$, Appl. Phys. Lett. 92 (2008) 102907.
[9] P. Scherrer, Bestimmung der grösse und der inneren struktur von kolloidteilchen mittels Röntgenstrahlen, Nachr. Ges. Wiss. Goettingen. 26 (1918) 98–100.
[10] D. Balzar, N. Audebrand, M.R. Daymond, A. Fitch, A. Hewat, J.I. Langford, A. Le Bail, D. Louer, O. Masson, C.N. McCowan, N.C. Popa, P.W. Stephens, B.H. Toby, Size–strain line-broadening analysis of the ceria round-robin sample, J. Appl. Cryst. 37 (2004) 911–924.
[11] P. Scardi, M. Leoni, R. Delhez, Line broadening analysis using integral breadth methods: a critical review, J. Appl. Cryst. 37 (2004) 381–390.
[12] C.T. Chantler, N.A. Rae, C.Q. Tran, Accurate determination and correction of the lattice parameter of LaB_6 (standard reference material 660) relative to that of Si (640b), J. Appl. Cryst. 40 (2006) 232–240.
[13] T.H. de Keijser, E.J. Mittemmeijer, H.C.F. Rozendaal, The determination of crystallite-size and lattice-strain parameters in conjunction with the profile-refinement method for the determination of crystal structures, J. Appl. Cryst. 16 (1983) 309–316.
[14] G.K. Williamson, W.H. Hall, X-ray line broadening from filed aluminum and wolfram, Acta Metall. 1 (1953) 22–31.
[15] I.D. Brown, The Chemical Bond in Inorganic Chemistry, Oxford University, Oxford, 2002.
[16] I.D. Brown, VALENCE: a program for calculating bond valence, J. Appl. Cryst. 29 (1996) 479–480.
[17] I.B. Bersuker, Modern aspects of the Jahn–Teller effect theory and applications to molecular problems, Chem. Rev. 101 (2001) 1067–1114.
[18] Y.-I. Kim, E. Lee, Constant-wavelength neutron diffraction study of perovskite oxynitrides $BaTaO_2N$ and $BaNbO_2N$, J. Ceram. Soc. Jpn. 119 (2011) 371–374.